Above-threshold ionization and high-order harmonic generation by mid-infrared and far-infrared laser pulses

Chengpu Liu, Takashi Nakajima,* Tetsuo Sakka, and Hideaki Ohgaki
Institute of Advanced Energy, Kyoto University, Gokasho, Uji, Kyoto 611-0011, Japan
(Received 19 December 2007; published 21 April 2008)

We investigate above-threshold ionization and high-order harmonic generation processes by mid-infrared (3.3 μm) and far-infrared (10 μm) laser pulses using the numerical solution of the time-dependent Schrödinger equation for the potassium atom. When the laser intensity is reasonably high, we find two plateaus in the above-threshold ionization spectra. With the use of two different potential models and a classical analysis, we clarify that the first plateau mainly originates from the contribution of the excited bound states while the second one is associated with the well-known backscattering process. Corresponding results for the harmonic spectra verify our interpretation.

DOI: 10.1103/PhysRevA.77.043411 PACS number(s): 32.80.Rm

I. INTRODUCTION

The interaction of an atom with an intense laser field has revealed various interesting phenomena. Among them above-threshold ionization (ATI) and high-order harmonic generation (HHG) are the most well known where the processes are highly nonlinear and nonperturbative [1,2]. Those phenomena have been extensively investigated from both theoretical and experimental aspects for more than a decade [3–5]. Note that the ATI and HHG processes are strongly related and complementary to each other, since the electron is eventually ejected in the former while it is eventually recombined with the core in the latter.

For an experimental as well as theoretical study of ultrafast laser-atom interactions, the combination of near-infrared laser pulses and rare gases is most commonly employed because of the availability of a Ti:sapphire-based fs laser system and the technical easiness to employ rare gases as a target [6–11]. The use of rare gases is also favorable in terms of the resistivity against ionization due to its high ionization potential. As a result, atoms can survive until the peak intensity without complete ionization, which is essential to observe highly nonlinear processes.

After the pioneering work by Sheehy *et al.* [12] who studied HHG by mid-infrared (3–4 μm) laser pulses using alkali-metal atoms as a target, there are several works reported for HHG as well as ATI by mid-infrared laser pulses [13,14]. As for far-infrared lasers, we find only a few works using CO_2 lasers in the early days [15–17]. Anyhow, the main difference between HHG and ATI in alkali-metal atoms by mid-infrared lasers and those in rare gases by near-infrared ($\sim$800 nm) lasers arises from the different atomic structure and the photon energy. It has been found that the first excited state of alkali-metal atoms plays a very important role. Moreover, it should be noted that, due to the participation of the excited bound states of alkali-metal atoms irradiated by mid-infrared lasers, application of the tunneling model to the alkali-metal atoms under mid-infrared lasers may not be as good as it is for rare gases under near-infrared lasers, as indeed found for HHG [12] and ATI [13,14]. For a better understanding of the interaction dynamics between atoms and mid- or far-infrared laser pulses, it is useful to investigate both ATI and HHG processes all the way down to the cutoff regions, which, however, requires tremendous numerical effort, in particular for the former: The use of mid- or far-infrared laser pulses implies that the propagation time becomes much longer compared with that for near-infrared laser pulses. Moreover, if we wish to assume a small Keldysh parameter the ponderomotive energy becomes rather large, which is another cause of computational difficulty since the interaction box size must be huge.

In this paper we investigate the interaction of alkali-metal (potassium) atoms with mid- and far-infrared laser pulses using a numerical solution of the time-dependent Schrödinger equation (TDSE). To circumvent the computational difficulty as we have explained above, we employ the one-dimensional (1D) TDSE. A classical analysis with the temporal pulse shape taken into account is also performed to interpret the numerical results. Furthermore, we study *both* ATI and HHG processes so that we can obtain complementary information. To our knowledge there is no work in the literature which has studied both ATI and HHG, in particular by mid- and far-infrared laser pulses. Our study for far-infrared laser pulses is also relevant since a compact free-electron laser is now under construction in our institute where the central wavelength lies in the mid- to far-infrared region [18,19].

II. METHOD

Our theoretical tool is a TDSE in the form of

$$i\frac{\partial\Psi(t)}{\partial t} = [H_0 + V(t)]\Psi(t). \tag{1}$$

H_0 is the field-free atomic Hamiltonian, and $V(t)$ is the time-dependent interaction between the electron and the laser field, which is defined by $V(t)=E(t)\hat{\varepsilon}\cdot\boldsymbol{r}$, with $E(t)$ being the electric field, $\hat{\varepsilon}$ the polarization vector, and $\boldsymbol{r}$ the position operator of the valence electron. The atomic units (a.u., $m=\hbar=e=1$) are used in all equations in this paper, unless oth-

*t-nakajima@iae.kyoto-u.ac.jp

erwise mentioned. For the following numerical calculations, we define the vector potential as

$$A(t) = A_0 f(t)\cos(\omega t + \Phi) = A_0 \sin^2\left(\frac{\pi t}{2\tau_p}\right)\cos(\omega t + \Phi). \tag{2}$$

Here A_0 is the peak amplitude of the vector potential and $f(t)$ the field envelope with the sine-squared shape instead of the Gaussian shape for the convenience of calculations. ω and Φ are the photon energy and the carrier-envelope phase (CEP), respectively. τ_p is a duration [full width at half maximum (FWHM)] of the pulse with the definition of $\tau_p = 2\pi N_p/\omega$, where N_p is a number of cycles of the pulse. From the vector potential, we obtain

$$E(t) = A_0\omega \sin(\omega t + \Phi) - A_0\frac{\partial f(t)}{\partial t}\cos(\omega t + \Phi). \tag{3}$$

Note that the second term in Eq. (3), which consists of the time derivative of the vector potential envelope, is negligible for many-cycle pulses, while it plays an important role for few-cycle pulses.

About the calculational procedure to obtain the ATI spectra, we have employed the methods described by Javanainen, Eberly, and Su [20]: The 1D TDSE is integrated in both time and space using the Crank-Nicholson method [21]. Since we use a box with a finite size, the continuum states are described as discrete (quasicontinuum) states. After the pulse is over, the photoelectron spectrum is computed by taking a projection of the total wave function onto the quasicontinuum wave functions, which are separately calculated by solving the "time-independent" Schrödinger equation without the laser field. To increase the smoothness of the ATI spectra, we have employed a linear interpolation for the quasicontinuum energies and averaged over four consecutive points. As for the HHG spectra, they are obtained by taking the fast Fourier transforms (FFT) of the dipole acceleration during the time propagation.

III. NUMERICAL RESULTS AND DISCUSSIONS

To describe the potassium atom, we employ the screened soft-core potential model [20] $V(x) = -1/\sqrt{\alpha^2 + x^2}$ and solve the 1D TDSE to obtain the ATI and HHG spectra. By setting α to 5.15, the ionization potential and the energies of the first and second excited states are calculated to be 4.34 eV and 1.49 and 2.37 eV from the ground state, respectively, which agree reasonably well with the experimental values of 4.34 eV and 1.61 and 2.61 eV for the potassium atom.

A. ATI spectra

Numerically solving the TDSE for an intense and very long laser pulse (such as ps) is very time consuming. Thus we decide to employ a short pulse duration in our study, which does not affect so much the generality of the conclusions. To start with, we assume a mid-infrared laser pulse. The laser wavelength and intensity we have chosen are $\lambda = 3.3$ μm and $I = 7\times10^{11}$ W/cm^2, respectively. The ponderomotive energy U_p and corresponding Keldysh parameter ($\gamma = \sqrt{I_p/2U_p}$) are about 0.73 eV and 1.72, respectively. I_p is the ionization potential. In Sec. III E, we study the case of far-infrared laser pulses.

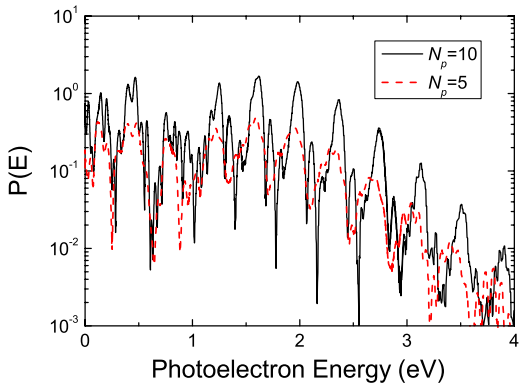

FIG. 1. (Color online) ATI spectra of the potassium atom irradiated by the mid-infrared laser pulse with two different pulse durations. The laser wavelength and peak intensity are 3.3 μm and 7×10^{11} W/cm^2, respectively. The pulse durations are chosen to be N_p=10 (~110 fs) (solid line) and N_p=5 (~55 fs) (dashed line).

Figure 1 shows the ATI spectra for two different pulse durations N_p=5 (~55 fs) and N_p=10 (~110 fs). The overall structure of the ATI spectra we show in Fig. 1 for the 1D TDSE agrees rather well with that for the 3D TDSE [13] except for the detailed substructures between the two consecutive main peaks. This can be mainly attributed to the difference of the level structure in the 1D and 3D models. The overall agreement between the 1D and 3D results justifies the use of the 1D model. Of course, depending on the physical quantities to look at, the limitation of the 1D calculation must be kept in mind if one is to quantitatively compare the 1D results with experimental data. The substructures between the main peaks come from either Freeman resonance [22] or Bardsley fringes [23]. The former is due to the dynamic resonance with Rydberg states. The latter is due to the interference of photoelectrons produced before and after the peak of the laser pulse, and sensitive to the pulse shape specifically chosen, such as sine-squared or Gaussian ones [24]. For the shorter laser pulse (N_p=5), the main peaks are broadened due to the laser bandwidth. For both pulse durations in Fig. 1, we find that the first several peaks are of comparable height, thus forming a *first* plateau in the ATI spectra [13], which is followed by a sharp cutoff at around $2.5U_p$.

Now, under the same laser parameters, the calculations are extended to the higher photoelectron energy region with a much larger spatial box until the cutoff appears. As clearly shown by the solid line in Fig. 2, we find a clear change of the slope in the ATI spectrum, which indicates that the backscattering process makes some contribution. As we increase the peak intensity from 7×10^{11} W/cm^2 (solid line in Fig. 2) to 1×10^{12} W/cm^2 (dashed line in Fig. 2), the presence of the *second* plateau becomes clear, which extends up to approximately 12.5 eV with a slowly decaying tail up to 17.5 eV. When the peak intensity increases further, the entire ATI spectrum (dot-dashed line in Fig. 2) shifts to the right due to

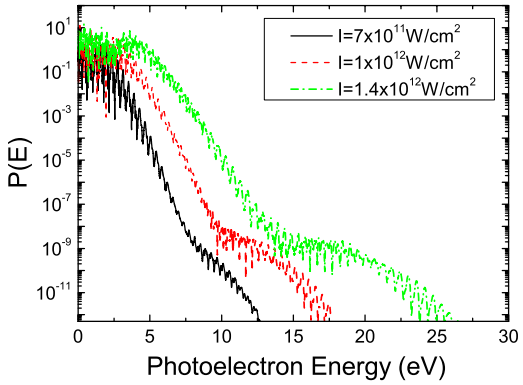

FIG. 2. (Color online) ATI spectra of the potassium atom irradiated by the 3.3 μm and $N_p=10$ ($\sim$110 fs) laser pulse. The peak intensities are chosen to be 7×10^{11} W/cm^2 (solid line), 1×10^{12} W/cm^2 (dashed line), and 1.4×10^{12} W/cm^2 (dot-dashed line), respectively.

the larger ponderomotive energy. We check the cutoff positions of the second plateaus and find that they are around 13 eV and 17 eV, respectively, which approximately agree with the cutoff energies given by the famous formula [25] $E_{\max}=10.007U_p+0.538I_p$ where the first term on the right-hand side is the classical cutoff value and the second term is the quantum modification. Of course, we should remember that the Keldysh parameter γ is still larger than unity for the peak intensities used in Fig. 2, which indicates that there must be a competition between the multiphoton and tunneling ionization processes.

Recall that the appearance of the first plateau is not very clear for the hydrogen atom as well as rare gases irradiated by near-infrared ($\sim$800 nm) laser pulses, although the minimum number of photons needed to reach the first excited state for the hydrogen atom at $\sim$800 nm does not differ so much from that for the potassium atom at $\lambda=3.3$ μm. In the following subsections we will study more in detail the physical origin of the two plateaus in terms of the HHG as well as ATI spectra.

B. Classical analysis

Although the classical theory of high-order ATI has been given in several papers (see Ref. [4] and references therein), most of the works assume a constant laser field [26] or an extremely short few-cycle pulse [5]. Our case—i.e., a several-cycle pulse—is just in between, and to be quantitatively more accurate, we now carry out a classical analysis with the temporal pulse shape taken into account. Briefly the classical theory can be summarized as follows [4,5,26]: Suppose that at time t_0 (ionization time) the electron is born at the origin with zero velocity. Subsequently the electron moves under the influence of the laser field with the binding potential completely ignored. After some time, the electron may return to the origin and an elastic backscattering with the core can take place at time t_r (backscattering time). After the backscattering, the electron moves in the laser field until time T_p when the laser field is turned off. After the termination of the laser pulse, the kinetic energy of the electron does not change anymore and the electron continues to fly toward the detector.

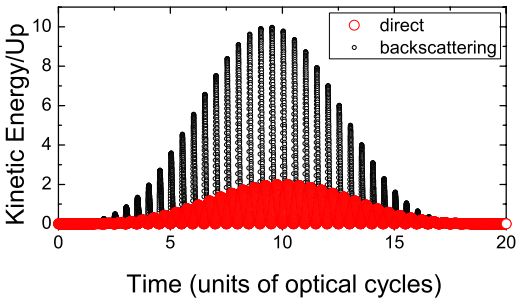

FIG. 3. (Color online) Classical results for the kinetic energy of photoelectrons. Solid and thin solid circles represent the direct and backscattering processes, respectively.

By solving Newton's equation $\ddot{r}(t)=-E(t)$, we obtain the electron velocity at any time after ionization, $t>t_0$, as $v(t)=A(t)-A(t_0)$. If the electron moves directly toward the detector without returning to the core (direct process), the final electron energy at the detector can be expressed as $[A(T_p)-A(t_0)]^2/2$. If the electron returns to the core under the laser field and elastically backscattered at time t_r (backscattering process), the following condition should be satisfied: $\int_{t_0}^{t_r}dt\, v(t)=0$. The final electron energy at the detector can be calculated to be $[A(T_p)-A(t_0)-v(t_r)]^2/2$.

In Fig. 3, we show the classical results for the kinetic energy of photoelectron for a wavelength of 3.3 μm and a peak intensity of 1.4×10^{12} W/cm^2, which are the same laser parameters employed for the calculation of the ATI spectrum (dot-dashed line in Fig. 2). The thick circles in Fig. 3 represent the direct process; i.e., once the electron has been freed through ionization, it does not return to the core. The thin circles in Fig. 3 represent the backscattering process. From Fig. 3, we find that the maximum kinetic energies of the electron which undergoes the direct and backscattering processes under the time-varying laser field are $2U_p$ and $10U_p$, respectively, which turn out to be practically the same with those for the constant laser field [26]. Therefore, although the corresponding Keldysh parameters are still slightly larger than unity, the second plateaus in Fig. 2 are clearly associated with the backscattering process. As for the first plateau, the cutoff position $2.5U_p$ is a little bit larger than $2U_p$ predicted by the classical analysis. Therefore, we suspect that the direct process may not be everything that contributes to the formation of the first plateau. Most likely it is the excited bound states that contribute to the formation of the first plateau. In the next subsection we will study in detail the effects of the excited bound states.

C. Effect of the excited bound states

In order to investigate the effect of the excited bound states, we now introduce a short-range potential [27] $V(x)=-\exp(-|x|)/\sqrt{\alpha^2+x^2}$ to represent the 1D potassium atom, which is similar to the Yukawa potential for the 3D calculation with a single-active-electron approximation [28]. Here α is chosen to be 1.87, which results in the same energy for the

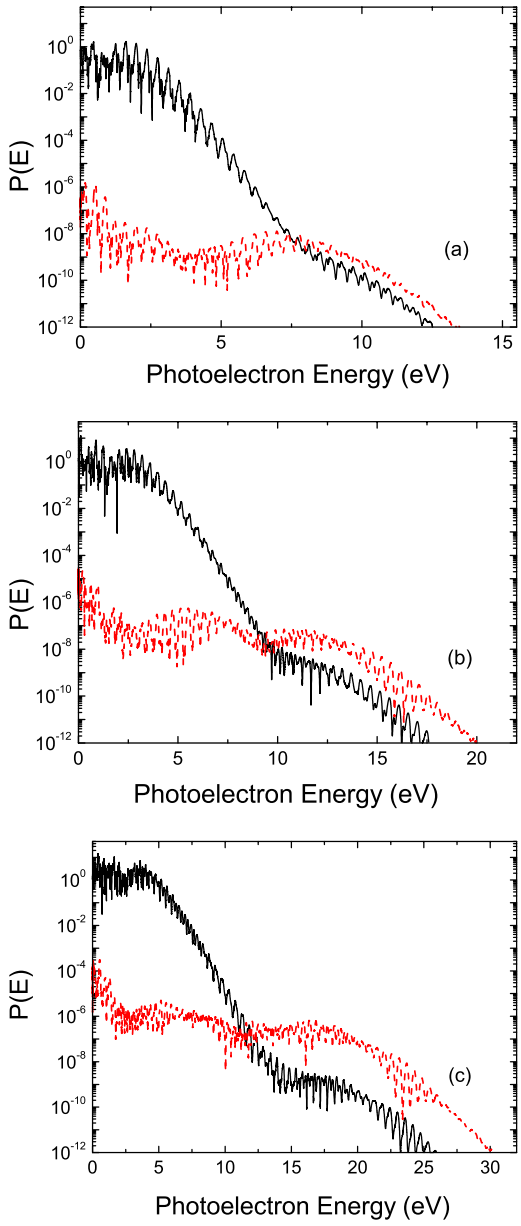

FIG. 4. (Color online) ATI spectra of the potassium atom irradiated by the 3.3 μm and $N_p=10$ ($\sim$110 fs) laser pulse for three different peak intensities: (a) 7×10^{11} W/cm^2, (b) 1×10^{12} W/cm^2, and (c) 1.4×10^{12} W/cm^2. In each graph, soft-core (solid line) and short-range (dashed line) potentials are employed for the calculations.

ground state of the potassium atom. Due to the short-range nature, this potential does not yield any excited bound states.

Under the same conditions we have employed for the three curves in Fig. 2 by the soft-core potential, we now calculate the ATI spectra by the short-range potential. The results are presented in Fig. 4 by both potentials at three different peak intensities. A careful examination of Figs. 4(a)–4(c) leads to the following observations: First, for the soft-core potential (solid lines), there exist two clear plateaus, while for the short-range potential (dashed lines) the plateau in the lower-energy domain disappears and only one plateau is left. The plateaus in the higher-energy domain have the similar cutoff energies for the two potentials, although the ionization efficiencies are quite different. This difference must come from the different backscattering probability which is determined by the ionization probability, atomic species, etc. Second, for the short-range potential, the first several ATI peaks decay rapidly toward $2U_p$ (which can be associated with the classical direct process), after which an almost flat plateau appears. Clearly this behavior is significantly different from that for the soft-core potential. From the comparison of the ATI spectra for the soft-core and short-range potentials, we speculate that the excited bound states play a crucial role for the formation of the first plateau. In order to gain more insights, we investigate the HHG spectra in the next subsection.

D. HHG spectra

We now calculate the HHG spectra by mid-infrared laser pulses using the two different potentials. The results are shown in Fig. 5 where the laser parameters have been chosen to be the same with those in Fig. 4 for the ATI spectra. The HHG spectra clearly show the general features of HHG: There exists a clear plateau followed by a long tail. The cutoff energy is consistent with the famous formula of $E_{\max}=3.17U_p+I_p$. With the increment of laser intensity, the cutoff energy naturally shifts to the higher harmonic orders. As we can clearly see in each panel of Fig. 5, we notice some differences between the results obtained for the two different potentials, although the cutoff energies turn out to be almost the same for both:

First, the conversion efficiency for the soft-core potential (solid lines in Fig. 5) is much larger than that for the short-range potential (dashed lines in Fig. 5). As we have mentioned before, the intensities we have chosen correspond to the transition regime between the multiphoton and tunneling ionization processes, and therefore there occurs a competition between them. For the case of the soft-core potential, the existence of the excited bound states enhances the ionization probability, which in return increases the recombination probability resulting in the higher high-order harmonic intensities. Second, the HHG spectra for the short-range potential reveal more distinct peaks than those for the soft-core potential, especially in the lower-order harmonics. Namely, the lower-order harmonics decay rapidly for the short-range potential, which is consistent with the perturbation theory. In contrast, they are almost constant for the soft-core potential. Of course, this difference can also be attributed to the effect of the excited bound states, since there are no excited bound states for the short-range potential. Recall that this argument is similar to that for the formation of the first plateau in the ATI spectra we have discussed in Sec. III C. Third, the intensities of the first-order harmonic (i.e., the elastic scattering of the fundamental laser field) for the two potentials are a little different. Remember that the choice of the potential parameters in the two different potentials to have the same ground-state energies does not guarantee that the spatial distributions of the wave functions are also the same. Actually, we find that they are very different (not shown here): The ground-state wave function for the short-range potential is

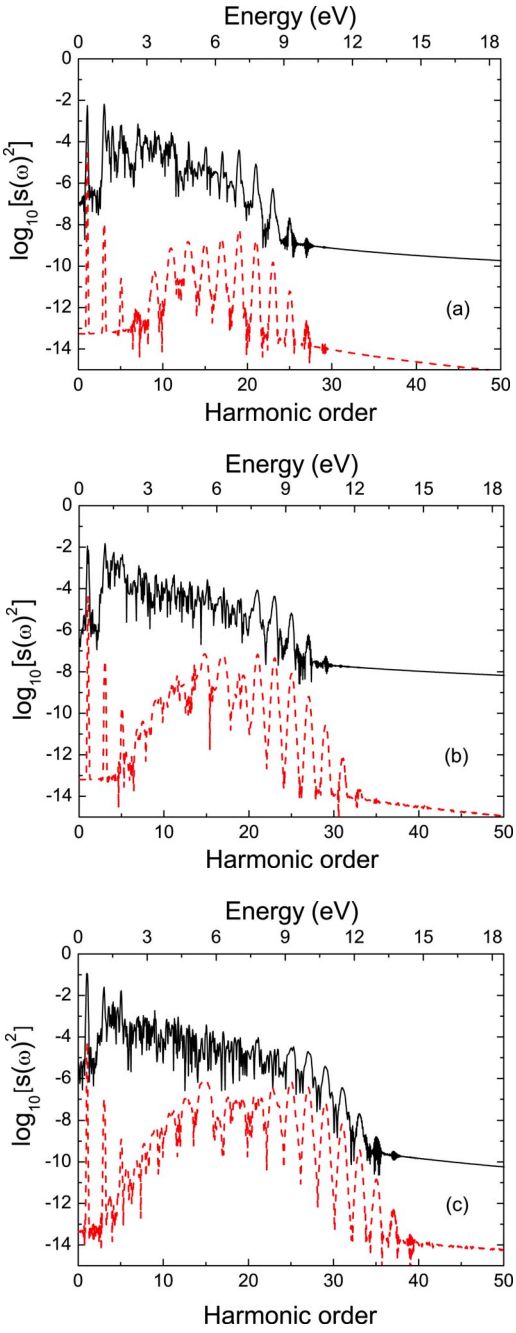

FIG. 5. (Color online) HHG spectra of the potassium atom under the same laser parameters used to calculate the ATI spectra in Fig. 4. In each graph, soft-core (solid line) and short-range (dashed line) potentials are employed for the calculations.

spatially narrower than that for the soft-core potential. Clearly, not only the excited bound states, but also the difference of the ground-state wave functions can significantly affect the HHG processes, since the recombination probability will be significantly affected when the ionized electron returns to the core. The last remark concerning Fig. 5 is that the difference of the HHG spectra by the two different potentials becomes smaller as the intensity increases from Fig. 5(a) to Fig. 5(c). This must be due to the fact that the contribution of the rescattered electron after the tunneling ionization processes directly from the ground state becomes

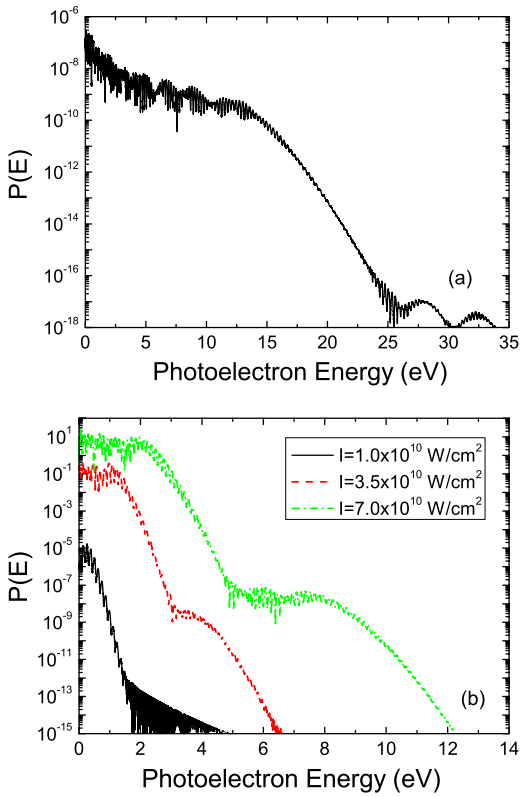

FIG. 6. (Color online) ATI spectra of the potassium atom irradiated by the far-infrared laser pulse. The laser wavelength and pulse duration are 10 μm and $N_p=5$ ($\sim$170 fs) for all graphs. (a) Atoms are initially in the ground state, and the peak intensity is $I=2.88\times10^{11}$ W/cm^2. (b) Atoms are initially in the *second excited state*, and the peak intensities are $I=1\times10^{10}$ (solid line), 3.5×10^{10} (dashed line), and 7.0×10^{10} (dot-dashed line) W/cm^2, respectively.

more dominant than that from the excited bound states as the intensity increases. We expect that the HHG spectra by the two potentials become even more similar at higher intensities since the excited states play lesser and lesser roles, although the difference originating from the different ground-state wave functions still remains regardless of the intensity.

E. Far-infrared excitation

Having investigated the ATI and HHG spectra by mid-infrared laser pulses, we now study the ATI spectra by far-infrared laser pulses. Figure 6(a) shows the ATI spectrum of potassium by far-infrared laser pulses. The laser wavelength, pulse duration, and peak intensity are, respectively, $\lambda=10$ μm, $N_p=5$ ($\sim$170 fs), and $I=2.88\times10^{11}$ W/cm^2, corresponding to the Keldysh parameter of $\gamma=0.9$ and the ponderomotive energy of $U_p=2.7$ eV. In Fig. 6(a) the presence of the plateaus is not clear due to the extremely small ionization efficiency. By increasing the laser intensity, however, the second plateau appears (not shown here) at the expense of significantly increased computation time due to the larger ponderomotive energy and the inherently long interaction time of the far-infrared laser pulse. To avoid this computational problem, we adopt an alternative method, without so

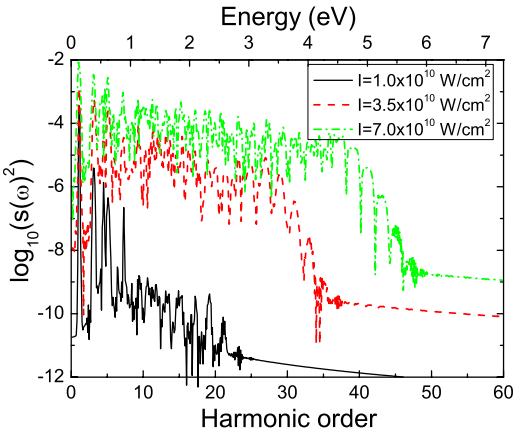

FIG. 7. (Color online) HHG spectra of the potassium atom irradiated by the far-infrared laser pulse. Atoms are initially in the *second excited state*, and the peak intensities are the same with those used to calculate the ATI spectra in Fig. 6(b).

much loss of generality, to study the behavior of the plateau and cutoff for far-infrared laser pulses: We assume that the initial state is not the ground state, but an excited state. Due to this choice of the initial state, the ionization efficiency is significantly increased for far-infrared lasers at moderate laser intensity, which is favorable to have a reasonably small ponderomotive energy, resulting in a much shorter computation time. Figure 6(b) shows the ATI spectra *from the second excited state* of the potassium atom for three different laser intensities $I=1\times10^{10}$, 3.5×10^{10}, and 7.0×10^{10} W/cm^2, corresponding to the Keldysh parameters and ponderomotive energies of $\gamma=3.2$ and $U_p=0.094$ eV, $\gamma=1.72$ and $U_p=0.33$ eV, and $\gamma=1.22$ and $U_p=0.66$ eV, respectively. At the intensity of $I=1.0\times10^{10}$ W/cm^2 [solid line in Fig. 6(b)], the ATI spectrum rapidly decays without forming a plateau. This implies that the ionization process is in the perturbation regime and direct or backscattering processes hardly occur. As the intensity is increased to 3.5×10^{10} W/cm^2 [dashed line in Fig. 6(b)], tunneling ionization sets in, and as a result both direct and backscattering processes take place with some probability, resulting in the formation of the first and second plateaus. At the higher intensity, $I=7.0\times10^{10}$ W/cm^2 [dot-dashed line in Fig. 6(b)], the presence of the plateaus becomes even more obvious. In Fig. 7 we present the HHG spectra at three different intensities which are chosen to be the same with those for the ATI spectra in Fig. 6(b). At low intensity (solid line in Fig. 7), only several low-order harmonics rapidly decay and no clear plateau is formed due to the same reason given above for the corresponding ATI spectrum. As the intensity increases (dashed and dot-dashed lines in Fig. 7), the presence of the plateaus becomes obvious. The cutoff of the plateau shifts toward the higher harmonics orders with the further increment of intensity.

F. Ionization for different photon energies

In the above, we have investigated the ATI and HHG spectra irradiated by mid- and far-infrared laser pulses and found that the excited bound states play an important role in the dynamics. The question we address now is how the importance of the excited bound states depends on the photon energy.

In Table I we list the ionization probabilities of the hydrogen and potassium atoms for different photon energies and intensities. Note that we have chosen different laser intensities so that the Keldysh parameter takes the same value—i.e., $\gamma=1.22$—for all cases. Recall that the same Keldysh parameter implies that, regardless of the atomic species, laser intensity, and photon energy, the ionization dynamics are similar. In order to see how much ionization actually takes place *directly from the initial state* we compare the results obtained by the soft-core potential and the dc tunneling ionization formula, which are represented by P_{sc} and P_{dc}, respectively. For comparison, we also list the ionization yield by the short-range potential P_{sr}. Now we may approximate the contribution of the excited bound states for ionization by $P_{sc}-P_{dc}$. For the hydrogen atom irradiated by the 800-nm laser pulse, the probability difference between P_{sc} and P_{dc} is about factor of 17, while that for K irradiated by the 3.3 μm laser pulse is about factor of 39 and that for K_s irradiated by the 10 μm laser pulse is about factor of 59. This indicates that, at least around the Keldysh parameter close to unity, the excited bound states play more important roles during the ionization process if the photon energy is smaller. We explain this trend as follows: During the rising time of the laser pulse, the excited states are populated through multiphoton absorption, and as the pulse approaches the peak intensity, tunneling

TABLE I. Ionization probabilities calculated for different atoms and photon energies at the intensities corresponding to the same Keldysh parameter, $\gamma=1.22$. H and K represent the hydrogen and potassium atoms, respectively, with an assumption that the atoms are initially in the ground states, while K_s represents the potassium atom with an assumption that the atoms are initially in the *second excited state*. I_p is the energy difference between the initial state and the ionization threshold, and N is the minimum number of photons needed for ionization. P_{sc} and P_{sr} are the ionization probabilities calculated for the soft-core and short-range potentials, respectively, while P_{dc} represents the dc tunneling ionization probability for the Coulomb potential.

Atoms	λ (μm)	I_p (eV)	N	I (W/cm^2)	γ	P_{sc}	P_{dc}	P_{sr}
H	0.8	13.6	9	7.5×10^{13}	1.22	5.24×10^{-2}	3.11×10^{-3}	3.66×10^{-4}
K	3.3	4.34	12	1.4×10^{12}	1.22	0.43	1.1×10^{-2}	3.67×10^{-6}
K_s	10	1.97	16	7.0×10^{10}	1.22	0.44	8.4×10^{-3}	3.3×10^{-9}

ionization takes place very easily from there. Therefore the ionization probability significantly increases through the excited bound states rather than directly from the initial state. Of course the excited bound states should play a lesser role if the intensity is further increased.

IV. CONCLUSIONS

In conclusion, we have theoretically studied the ATI and HHG processes in the potassium atom by intense mid-infrared (3.3 μm) and far-infrared (10 μm) laser pulses by numerically solving the time-dependent Schrödinger equation. We have found that the excited bound states play very important roles for both ATI and HHG processes.

One of the most eminent strong field phenomena in alkali-metal atoms irradiated by mid- and far-infrared laser pulses is the formation of two plateaus in the ATI spectra. Through the classical analysis with a temporal pulse shape taken into account, we have ensured that, for both mid- and far-infrared laser pulses, the first plateau in the low-energy region is associated with the direct process, while the second plateau in the high-energy region is associated with the well-known backscattering process of ionized electrons. The maximum energy of the first plateau, however, does not exactly agree with the highest kinetic energy predicted by the classical theory for the direct process. This indicates that the atomic structure, which is often totally neglected in both classical and quantum analysis based on tunneling ionization, plays some role, in particular for the low-energy photoelectrons. In contrast, the cutoff energy of the second plateau is consistent with the well-known cutoff law. We have further verified our interpretation by carrying out quantum mechanical calculations using the two different potentials—i.e., the soft-core and short-range potentials—and found that the excited bound states play a crucial role for the formation of the first plateau. Closely related to the ATI spectra by mid- and far-infrared laser pulses, we have found a similar enhancement in the HHG spectra due to the excited bound states, as we have expected.

As a last remark, we would like to note that, even if the Keldysh parameter takes the same value (which is close to unity in our specific study), the importance of the excited bound states in the strong field dynamics can be quite different for different atoms, initial states, and photon energies under appropriate intensities, since the contribution of the excited bound states cannot be totally neglected in a realistic situation.

ACKNOWLEDGMENTS

C.L. acknowledges financial support from the Japan Society for the Promotion of Sciences (JSPS) and the hospitality at Kyoto University during his stay. The work by T.N. was supported by a Grant-in-Aid for scientific research from the Ministry of Education and Science of Japan.

[1] P. Agostini, F. Fabre, G. Mainfray, G. Petite, and N. K. Rahman, Phys. Rev. Lett. **42**, 1127 (1979).
[2] A. L'Huillier and Ph. Balcou, Phys. Rev. Lett. **70**, 774 (1993).
[3] T. Brabec and F. Krauze, Rev. Mod. Phys. **72**, 545 (2000).
[4] W. Becker, F. Grasbon, R. Kopold, D. B. Milosevic, G. G. Paulus, and H. Walther, Adv. At., Mol., Opt. Phys. **48**, 35 (2002).
[5] D. B. Milosevic, G. G. Paulus, D. Bauer, and W. Becker, J. Phys. B **39**, R203 (2006).
[6] Z. Chang, A. Rundquist, H. Wang, M. M. Murnane, and H. C. Kapteyn, Phys. Rev. Lett. **79**, 2967 (1997).
[7] M. Schnurer, Ch. Spielmann, P. Wobrauschek, C. Streli, N. H. Burnett, C. Kan, K. Ferencz, R. Koppitsch, Z. Cheng, T. Brabec, and F. Krausz, Phys. Rev. Lett. **80**, 3236 (1998).
[8] B. Yang, K. J. Schafer, B. Walker, K. C. Kulander, P. Agostini, and L. F. DiMauro, Phys. Rev. Lett. **71**, 3770 (1993).
[9] G. G. Paulus, W. Nicklich, H. Xu, P. Lambropoulos, and H. Walther, Phys. Rev. Lett. **72**, 2851 (1994).
[10] G. G. Paulus, W. Nicklich, and H. Walther, Europhys. Lett. **27**, 267 (1994).
[11] F. Grasbon, G. G. Paulus, H. Walther, P. Villoresi, G. Sansone, S. Stagira, M. Nisoli, and S. De Silvestri, Phys. Rev. Lett. **91**, 173003 (2003).
[12] B. Sheehy, J. D. D. Martin, L. F. DiMauro, P. Agostini, K. J. Schafer, M. B. Gaarde, and K. C. Kulander, Phys. Rev. Lett. **83**, 5270 (1999).
[13] P. Maragakis, E. Cormier, and P. Lambropoulos, Phys. Rev. A **60**, 4718 (1999).
[14] M. B. Gaarde, K. J. Schafer, K. C. Kulander, B. Sheehy, Dalwoo Kim, and L. F. DiMauro, Phys. Rev. Lett. **84**, 2822 (2000).
[15] P. B. Corkum, N. H. Burnett, and F. Brunel, Phys. Rev. Lett. **62**, 1259 (1989).
[16] C. Y. Tang, P. G. Harris, A. H. Mohagheghi, H. C. Bryant, C. R. Quick, J. B. Donahue, R. A. Reeder, Stanley Cohen, W. W. Smith, and J. E. Stewart, Phys. Rev. A **39**, 6068 (1989).
[17] F. A. Ilkov, T. D. G. Walsh, S. Turgeon, and S. L. Chin, Phys. Rev. A **51**, R2695 (1995).
[18] H. Ohgaki, I. Tometaka, K. Yamane, T. Kii, K. Masuda, K. Yoshikawa, and T. Yamazaki, Nucl. Instrum. Methods Phys. Res. A **507**, 150 (2003).
[19] H. Zen, T. Kii, K. Masuda, H. Ohgaki, and T. Yamazaki, Infrared Phys. Technol. (to be published).
[20] J. Javanainen, J. H. Eberly, and Q. Su, Phys. Rev. A **38**, 3430 (1988).
[21] W. H. Press, B. P. Flannery, S. A. Teukolsky, and W. T. Vetterling, *Numerical Recipes: The Art of Scientific Computing* (Cambridge University Press, Cambridge, England, 1986).
[22] R. R. Freeman, P. H. Bucksbaum, H. Milchberg, S. Darack, D. Schumacher, and M. E. Geusic, Phys. Rev. Lett. **59**, 1092 (1987).
[23] J. N. Bardsley, A. Szoke, and M. J. Comella, J. Phys. B **21**, 3899 (1988).
[24] Chengpu Liu and Takashi Nakajima (unpublished).

[25] M. Busuladzic, A. Gazibegovic-Busuladzic, and D. B. Milosevic, Laser Phys. **16**, 289 (2006).
[26] G. G. Paulus, W. Becker, W. Nicklich, and H. Walther, J. Phys. B **27**, L703 (1994).
[27] W. G. Greenwood and J. H. Eberly, Phys. Rev. A **43**, 525 (1991).
[28] Chengpu Liu and Takashi Nakajima, Phys. Rev. A **76**, 023416 (2007).